Computational Aerodynamic Analysis of a Tension Cone Supersonic Inflatable Aerodynamic Decelerator

Ian G. Clark, Robert D. Braun
Guggenheim School of Aerospace Engineering
Georgia Institute of Technology
Atlanta, GA 30332-0150
ian.clark@gatech.edu

Abstract—The 2009 Mars Science Laboratory mission has brought renewed awareness to the difficulty of landing large payloads on the surface of Mars. As a result, a new suite of decelerator technologies is being investigated for future robotic and human-precursor missions. One such technology is the supersonic inflatable aerodynamic decelerator (IAD). Previous studies have shown that a supersonic IAD can provide sizable increases in landed mass versus traditional parachute based systems, particularly for near-term robotic mission. This is due to the ability of an IAD to deploy at higher Mach numbers and dynamic pressures than a parachute, thus allowing for greater deceleration earlier in the entry sequence. [1][2]

As part of the Program to Advance Inflatable Decelerators for Atmospheric Entry, one particular configuration, the tension cone, has undergone a series of wind tunnel experiments designed to acquire a full characterization of the aerodynamic performance of a particular tension cone geometry. One test objective entailed the acquisition of a data set useful for validating computational tools for later IAD analysis efforts.

This paper presents a summary of the work performed in investigating two separate computational fluid dynamics codes for their suitability in predicting tension cone performance. The first code, NASCART-GT, is a solution-adaptive, Cartesian grid code that is used for rapid inviscid analysis of axisymmetric geometries. The second code, Overflow was used for Navier-Stokes analysis of three-dimensional geometries. These codes were evaluated for their ability to match measured pressure distributions, static force and moment coefficients, and observed flowfield characteristics. Overflow is also used to investigate flow features that were not observed during testing, such as the aft body recirculation region.

Additional investigation into the aerodynamic performance of a tension cone was performed through a parametric analysis of multiple tension cone geometries. Three primary shape parameters were varied with the goal of identifying undesirable flowfield characteristics such as shocks attached to the surface of the tension shell and to provide insight into the sensitivity of drag to tension cone geometry.

1. INTRODUCTION

In the summer of 2011, the Mars Science Laboratory (MSL) mission will seek to place an 850 kg rover on the surface of Mars. This landing will rely on two Viking-era technologies that have been the mainstay of Mars entry, descent, and landing, namely rigid 70º sphere-cone aeroshells and disk-gap-band (DGB) parachutes. The 850 kg MSL rover likely represents the limit in landed mass that is possible with these technologies [1]. Constraints in launch vehicle fairings limit the size of rigid aeroshells while parachutes are constrained by limits in Mach number and dynamic pressure during deployment. Future Mars missions that seek to land payloads exceeding 850 kg will require lower ballistic coefficients, and thus larger drag areas, earlier in the entry phase than is presently possible with the current state of the art of decelerator technology.

The MSL mission has brought renewed awareness to the difficulty of landing large payloads on Mars and a new suite of decelerator technologies is being investigated for maturation. One such technology is the supersonic inflatable aerodynamic decelerator (IAD). Compared to hypersonic IADs that are traditionally envisioned as deploying prior to atmospheric entry, supersonic IADs are exposed to considerably lower heating and deceleration loads and may represent a more tractable solution for near-term Mars missions. A prior study on the use of a supersonic IAD has estimated that improvements of as much as 80% in payload mass are possible when a supersonic IAD is employed [2].

One candidate IAD configuration is the tension cone, shown in Figure 1. This type of IAD consists of an axisymmetric, single-surface membrane attached at one end to the entry vehicle's aeroshell and at the other end to an inflated torus. The curvature of the shell portion is uniquely designed so as

to exhibit only tensile stresses for an assumed pressure loading.

Figure 1. Tension cone inflatable aerodynamic decelerator.

Recently, as part of the Program to Advance Inflatable Decelerators for Atmospheric Entry (PAIDAE), the tension cone underwent several wind tunnel tests. These tests sought to characterize the aerodynamic performance of a particular configuration in the supersonic regime. Testing conducted on rigid models provided static aerodynamic force and moment coefficients, surface pressure distributions, and characterization of the flow field around the test article. Testing was also conducted on flexible, deployable models in an effort to investigate the deployment mechanics of the tension cone as well as the pressures required in the inflatable torus. In addition to aerodynamic performance evaluation, the wind tunnel tests had the primary objective of attaining data useful for the validation of computational tools capable of predicting decelerator performance.

The future design and development efforts of supersonic IADs will rely heavily on computational analyses to accurately assess performance characteristics. With this in mind, a study was undertaken to explore the current capacity of computational codes to accurately model basic tension cone aerodynamics. This paper presents work performed in analyzing computational fluid dynamics tools with differing degrees of fidelity. The results attained from this research are used to provide additional insights into the flowfield surrounding the tension cone. In addition, a parametric investigation of tension cone configurations is performed in an effort to address shape optimization for increased drag and flowfield stability. The research outlined in this paper takes a necessary first step in analyzing coupled aerodynamic-structural analyses by first exploring and validating the static aerodynamics on rigid configurations.

2. EXPERIMENTAL SUMMARY

Wind tunnel testing conducted on rigid tension shell models was conducted at the 4- x 4-foot Langley Unitary Wind Tunnel. Testing was conducted on two different models, a force and moment model and a pressure model. The force and moment model was integrated with a six-component wind tunnel balance and used to attain static aerodynamic characteristics including force and moment coefficients. A profile of the model assembly is shown in Figure 2. The outer mold line directly behind the tension cone corresponds to the balance windshield, commonly used in wind tunnel

testing to prevent the balance from measuring loads other than those directly on the model.
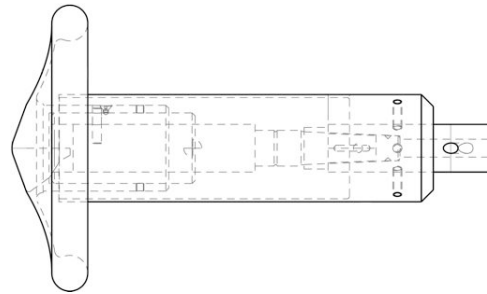

Figure 2. Wind tunnel model assembly of the force and moment model.

Dimensionally, the force and moment and pressure models were identical and were 6-inches in diameter, corresponding to a 1.07% scale model of a 4.5 m diameter aeroshell employing a tension cone IAD. The complete model assembly outer mold line, including sting and windshield, was also kept as similar as possible with the exception that a different sting was required for the pressure model. The pressure model contained 82 pressure ports, arranged in three spokes of 27 ports plus one port at the nose. Included among the 27 ports were four ports on the backside of the pressure model, two on the torus and two on the backside of the tension shell. The radial distribution of the ports, shown in Figure 3, was derived based upon a predicted pressure distribution.
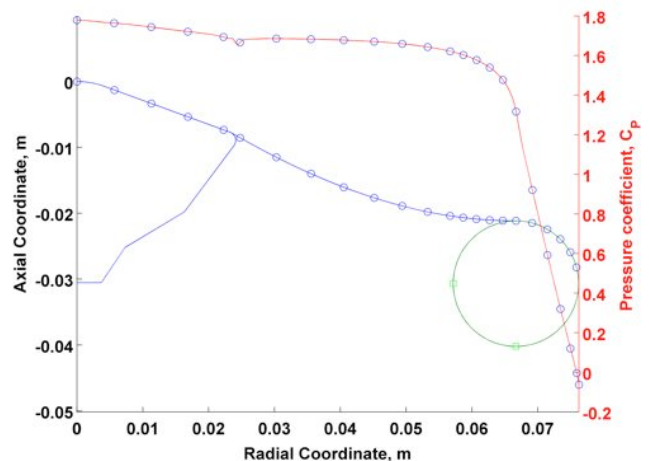

Figure 3. Radial distribution of the tension cone pressure ports.

The three spokes were located at 0º, 90º, and 225º positions. Because the model could be rolled 180º, these three spokes effectively allowed for pressure readings at locations 45º apart. Three additional pressure ports were located at the base of the windshield and pressures were recorded during both force and moment and pressure model testing. The purpose of these ports was to measure the windshield cavity pressure, which was used during data reduction procedures.

Force and moment testing was conducted using Langley balance 2008, a six-component strain gauge balance. The pressure model required use of an additional 82 pressure transducers. The transducers consisted of a mix of 5 psi and 15 psi ESP modules. The 5 psi modules were used for the aftbody pressures and the pressure ports located at the periphery of the model. All other ports utilized 15 psi ESP modules. Data acquisition for the force and moment model was performed at a sampling rate of 30 Hz over a duration of 2 seconds. This duration was extended to 15 seconds during pressure model testing. Recorded values were an average of the sampled values. Settling times of 10 seconds for the force and moment testing and 30 seconds for the pressure testing were used in between each data point.

Data were attained at Mach numbers of 1.65, 2.0, 2.5, 3.0, 3.5, and 4.5, with each Mach number including several angles of attack and angles of sideslip. Results shown in this paper are for a model Reynolds number of 10^6 based on the maximum diameter of the model.

The results from the testing of the rigid models are presented in subsequent sections alongside those attained from CFD.

3. INVISCID COMPUTATIONAL ANALYSES

Prior studies on tension cone aerodynamics have definitively demonstrated that simple Newtonian impact methods are unsuitable for accurate prediction of surface pressures [3],[4]. Pressure distributions derived using integral-relation theory [5] have shown reasonable accuracy for several variants of the tension cone [4]. However, this method appears to be limited in the types of geometries and conditions for which it is suitable [5]. In particular, low Mach number conditions and geometries with concave surfaces produced less accurate results. One possible alternative for providing rapid analysis of tension cone geometries would be to use inviscid aerodynamics tools. Since drag on blunt bodies at supersonic conditions is dominated by pressure forces (versus viscous shear forces) it is expected that inviscid aerodynamics should be able to provide a reasonable estimation of drag performance and basic flow field characteristics. Though it is recognized that Euler aerodynamics would likely be unsuitable for detailed design efforts, this portion of the investigation was aimed at ascertaining their suitability for preliminary analysis purposes.

Inviscid analysis of the tension cone was performed using the NASCART-GT code [6],[7]. NASCART-GT is a solution-adaptive, Cartesian grid based analysis tool that provides automated generation of grids around axisymmetric, two-dimensional, or three-dimensional geometries. For this reason, it is particularly well-suited for providing rapid estimates of tension cone drag characteristics. Though capable of providing viscous analysis in the form of coupled Euler-integral boundary layer methods or full Navier-Stokes methods, for this effort NASCART-GT was only utilized for inviscid, axisymmetric analysis.

Grid Development and Setup

Though NASCART-GT provides automated grid generation, several parameters are required for control of the grid resolution. Control of the minimum cell size is achieved through specification of the fewest number of surface grid points to place along the longest body dimension. For the current analysis a value of 256 was used, resulting in the mesh shown in Figure 4. This value was seen to be sufficient to capture the general shape of the geometry and to resolve the detached bow shock but insufficient to capture minute details such as the small tension shell/aeroshell interface.
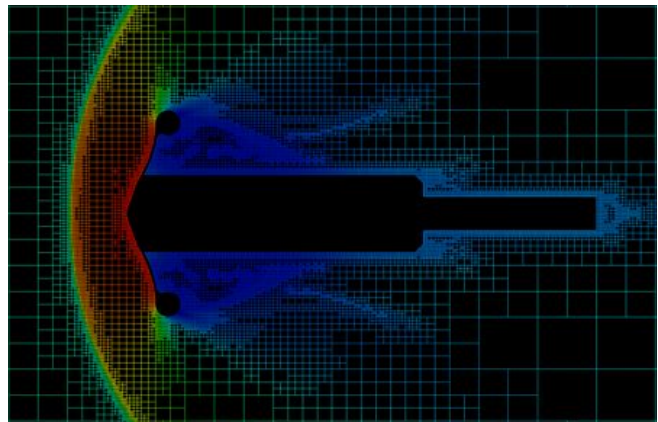

Figure 4. Computational mesh used for axisymmetric, inviscid analysis.

Solutions were computed for a total of 5000 iterations, which was seen to be sufficient to lower residuals by at least four orders of magnitude. Computational time was less than 20 minutes per case on a 3.0 GHz Intel processor. Calculation of inviscid fluxes was limited to first order accuracy.

Pressure Distribution Results

Provided in Figure 5 and Figure 6 are the surface pressures predicted by inviscid analysis and those measured in the wind tunnel. Good agreement is visible across a majority of the surface. The largest deviations are seen to occur along the shoulder and aftbody regions, areas where viscous effects are more dominant. The inviscid calculations overestimate the pressure along the shoulder and tend to underestimate the aftbody pressures. Overestimation of the shoulder pressures may be due to the first order accuracy employed and the large degree of damping provided as a result. That is, the solution may be overdamped and accurate expansion of the flow around the shoulder, and the subsequent decrease in pressure, is not achieved. An anomaly in estimated pressure is noted near the centerline location, where the pressure is seen to dip right at the stagnation point region. This is attributed to the solution being axisymmetric and the stagnation point lying at what is

essentially a single node point, introducing numerical difficulties. This anomaly may also be responsible for predicted pressures within 20 mm of the nose being consistently lower than what was measured.
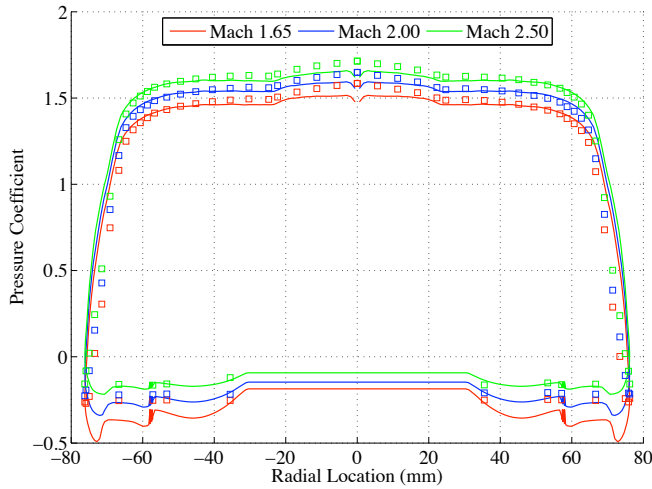

Figure 5. Inviscid predicted and measured surface pressures at 0° AoA and Re = 10⁶ (solid lines correspond to CFD data, squares to wind tunnel data).
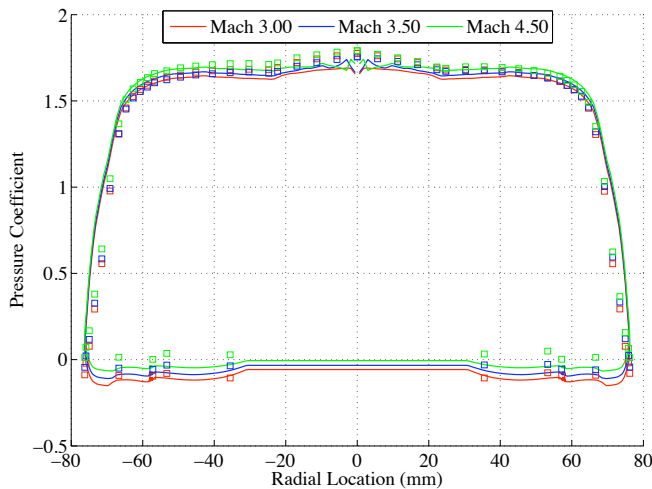

Figure 6. Inviscid predicted and measured surface pressures at 0° AoA and Re = 10⁶ (solid lines correspond to CFD data, squares to wind tunnel data).

Force and Moment Results

Figure 7 provides a comparison of the predicted 0° angle of attack drag coefficients and those measured during testing. Since surface pressures were seen to be reasonably close on the forebody but generally too low on the aft body, a forebody-only drag coefficient is also included for comparison.

The predicted values of total drag can be seen to be within 10% of the measured values. Computed estimates of total drag are seen to follow a different trend versus Mach number than those measured. In particular, the CFD estimates show less variation and predict drag to rise as the

Mach number approaches unity. In contrast, the forebody-only drag coefficients tend to be closer to measured values of drag coefficient. Furthermore, they more accurately capture the trend of decreasing drag coefficient with decreasing Mach number.
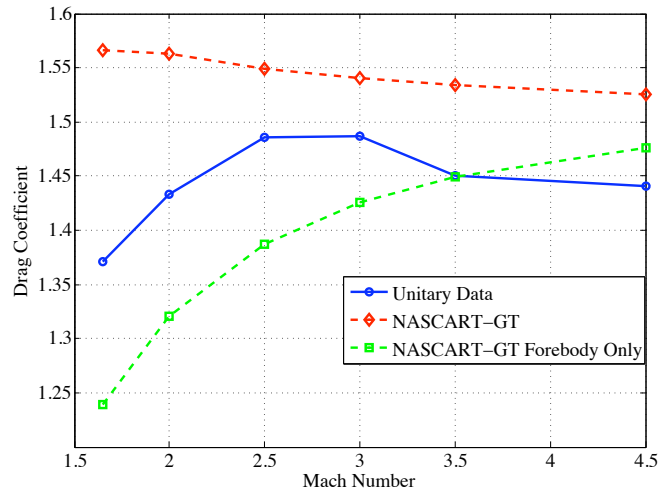

Figure 7. Comparison of wind tunnel data and inviscid CFD values of C_D at a 0° angle of attack and Re = 10⁶.

Flowfield Results

Figure 8 is a comparison of the shock structure calculated by NASCART-GT and that attained from Schlieren imagery. Vertical bars seen in the Schlieren image are windowpanes on the door to the wind tunnel test section. The computed solution provides excellent agreement in the location and curvature of the detached bow shock. However, other flow features such as the expansion and recompression details in the Schlieren image are not resolved as well. This is not unexpected since these are features whose location and shape can be influenced by viscous terms.
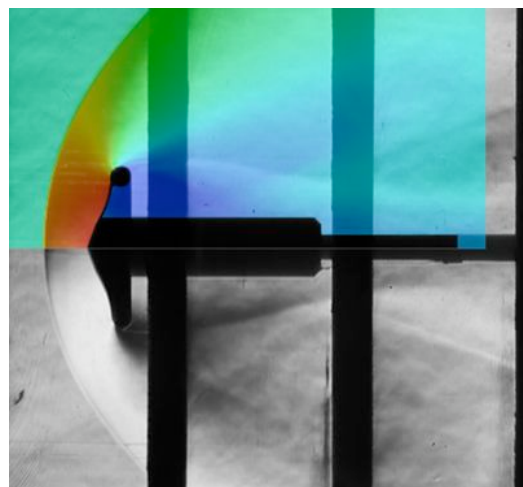

Figure 8. Comparison of shock structure at a 0° angle of attack for Mach 2.0 and Re = 10⁶.

4

4. VISCOUS COMPUTATIONAL ANALYSES

Future development of IADs will require accurate modeling of the device's aerodynamic performance. However, the codes used for this analysis must first demonstrate their suitability for these types of geometries. The objective of this portion of the research entailed the validation of a viscous CFD code for predicting the supersonic aerodynamics of a tension cone. In the context of this study, validation is considered to be a successful demonstration that the code can reproduce the results from prior wind tunnel testing.

Viscous CFD analysis was performed using the Navier-Stokes code Overflow [8]. Originally developed as a rewrite of the F3D/Chimera code, Overflow utilizes overset structured grids for near-body volumes and a Cartesian grid for off-body volumes. The overset approach has the advantage of simplifying the grid generation process since different grid blocks are not required to align with each other in any particular manner. This aspect allows for many of the grid generation processes to be scripted and performed in a more automated manner than typically possible, an approach taken in the current study.

Grid Development and Setup

The complete computational grid, shown in Figure 9, was constructed using 134 separate grids of varying size and resolution. Approximately 16 million grid points were used on a combination of structured body-fitted grids and Cartesian off-body grids. The solutions were computed using turbulent Navier-Stokes equations incorporating the three-equation Lag turbulence model [9], [10]. The Lag model is a modification of the basic two-equation turbulence model that adds a third equation to better model eddy viscosity. Grid spacing at the surface was calculated so as to produce a y+ parameter value of unity.

Solutions were computed in 16-processor parallel mode on NASA's Columbia Supercomputer for a total of 2000 iterations. Wall clock time generally ran between four and five hours per solution. Final residual values varied for each of the 139 grids used but were generally at least five orders of magnitude lower than for the first iteration.
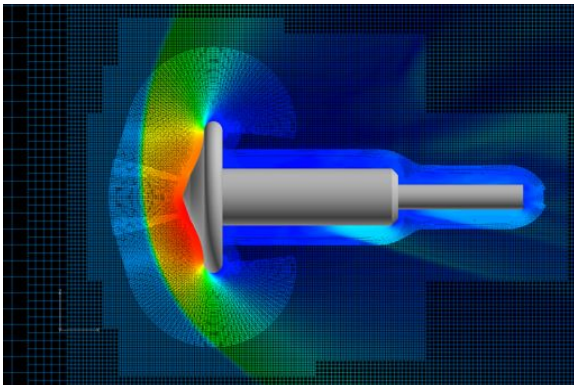

**Figure 9. Computational mesh used for viscous analysis.**

Pressure Distribution Results

Provided in Figure 10 are comparisons of the surface pressure distributions predicted by Overflow and those acquired from testing at three different Mach numbers. At the lower Mach numbers (<3.5), predicted pressures demonstrate excellent agreement with test values and the code was able to capture all the dominant trends in surface pressure. For those cases, significant improvement over the inviscid analyses was achieved for calculation of the shoulder and aftbody pressures.

The largest differences in values occurred for the 20º angle of attack solution near the windward -50 mm. radial location. At this angle of attack the stagnation point has moved from the conical portion of the sphere-cone forebody and onto the concave portion of the tension cone. Furthermore, much of the concave region is stagnant, as evidenced by the nearly constant high surface pressure. Examination of Figure 10c shows that the CFD solution tends to under predict the surface pressure in this region. Though still being investigated, this could be indicative of the code predicting a more turbulent boundary layer than otherwise occurred during testing. One recent study examining the use of the Lag model for analyzing blunt bodies at supersonic conditions has noted that the model tended to produce more unsteadiness than other models [11].

Another characteristic of the computed pressure distribution is the adverse pressure gradient seen at the sphere-cone/tension shell interface point (radial location of approximately 23 mm). Though a small dip in surface pressure was measured, the computed solution shows a slightly stronger pressure drop. This is likely due to a combination of the turbulence model and differences between the wind tunnel model geometry and that used for analysis. In particular, on the wind tunnel model the transition from a 70º sphere-cone to a 60º tension cone occurred smoothly along a shoulder with a radius of 1.3mm. On the computational model the transition was a sharp corner.

Beginning at a Mach number of 3.5 the predicted pressure distribution is seen to deviate significantly from the measured distribution. Although a 0º angle of attack solution provides good agreement, larger angles of attack exhibit major departures. In particular, the flow is predicted to separate in the region of the sphere-cone forebody. Though not shown, similar difficulties were observed in solutions calculated at Mach 4.5. The behavior was clearly not observed during testing and indicates a deficiency in the current modeling approach. Similar to the under predicted surface pressures, this is hypothesized to be due to the turbulence model incorrectly predicting transition much earlier than would naturally occur. Attempts at incorporating alternative turbulence models, e.g. the shear stress transport (SST) model, proved unsuccessful in eliminating this phenomenon.
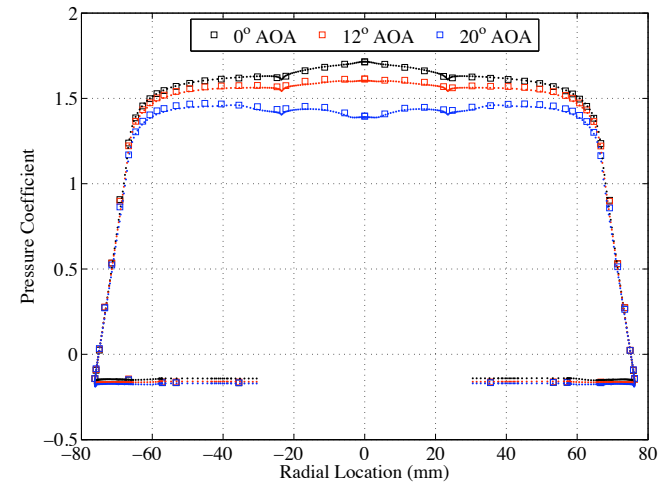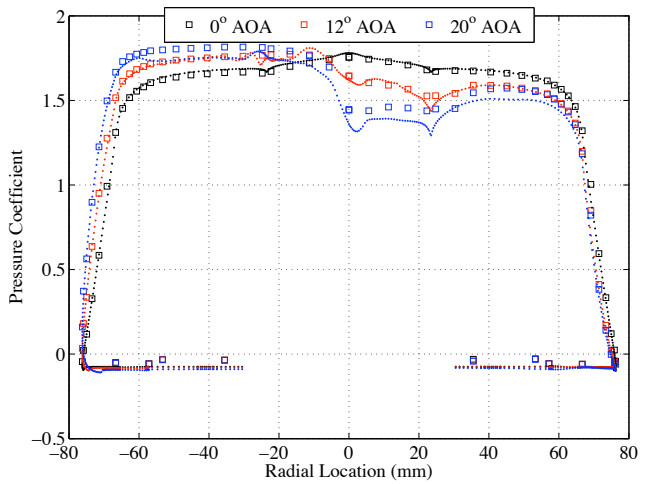
5
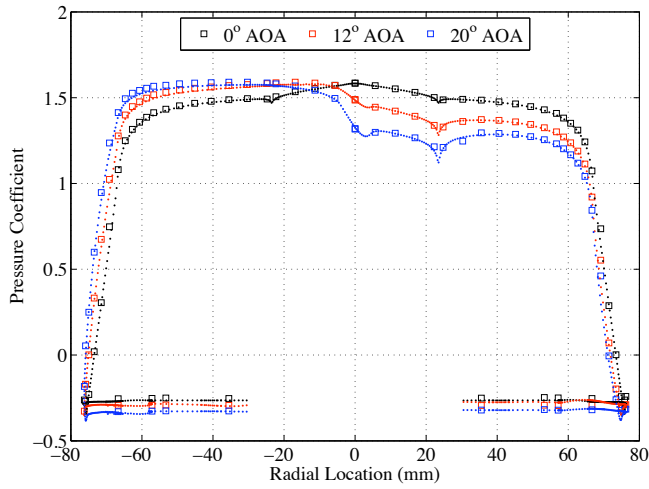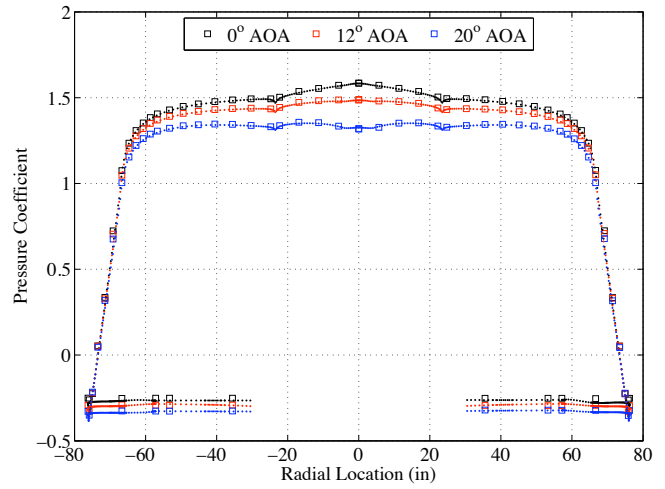
a) Mach 1.65, 0° Spoke
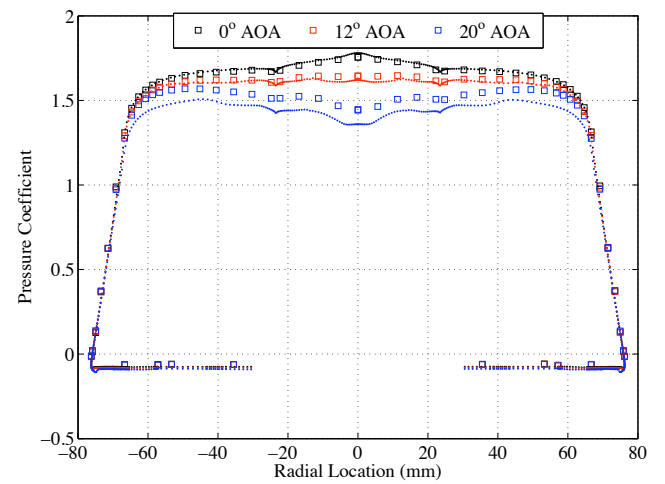
b) Mach 1.65, 90° Spoke
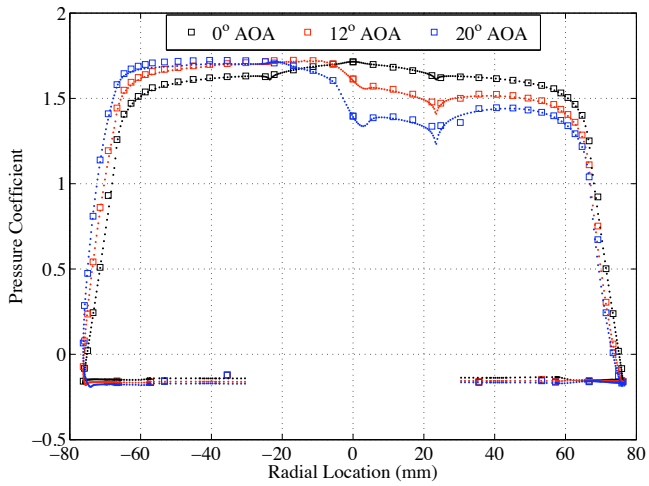
c) Mach 2.50, 0° Spoke

d) Mach 2.50, 90° Spoke

e) Mach 3.50, 0° Spoke

f) Mach 3.50, 90° Spoke

Figure 10. Surface pressure comparisons of wind tunnel results and Overflow predictions at Re = 10^6. Square data points correspond to wind tunnel data.
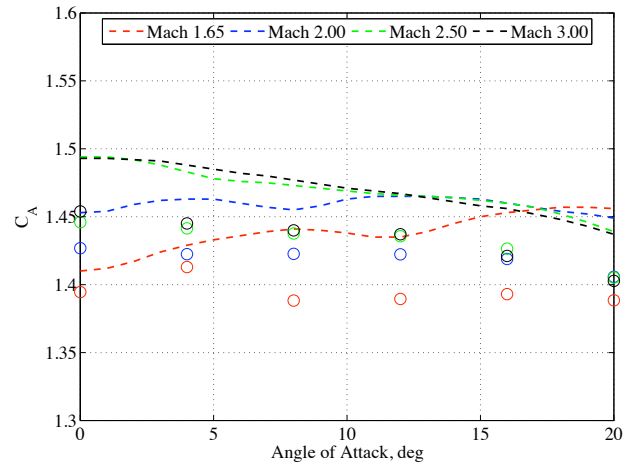
Force and Moment Results

A comparison of the force and moment coefficients calculated through CFD and those measured in the wind tunnel is provided in Figure 11. Only results up to Mach 3.0 are provided due to the separation issues encountered at higher Mach numbers. The largest discrepancies are observed with respect to the axial force coefficients. For the conditions analyzed, differences up to 4.5% were seen. However, though the disagreement in values is evident, the CFD results capture the same trends measured during testing, indicating that the data is likely only offset. In particular, the small oscillation versus angle of attack seen in the Mach 1.65 and Mach 2.0 cases is evident in both data sets. The proximity of the Mach 2.5 and Mach 3.0 solutions is also captured well. A likely explanation to the observed offset entails subtle differences between the wind tunnel test setup and the modeled geometry. Calculation of forces on the CFD model is limited to the forebody and the aftbody portion from windshield outwards. However, during testing, a small gap existed between the windshield and the back of the model and thus the balance was not completely isolated. Therefore, the forces reported by the balance likely include a small component due to the pressures inside the windshield cavity.

Examination of the normal force and pitching moment coefficient data shows very good agreement. Measurements of normal force were seen to include a very small dependence on Mach number. Although the Mach number dependence may well be within the uncertainty of the balance measurement, the computed CFD solutions also predicted a small variation, particularly at larger angles of attack. Measurements of pitching moment (referenced to the nose of the model) showed no variation versus Mach number, a characteristic also captured by the CFD solutions.

Flow Field Results

Figure 12 provides an overlap of the predicted density contours for a 20° angle of attack, Mach 2.0 test condition against a Schlieren image acquired at the same condition. Shock structure as seen in the Schlieren image is emphasized by a thin red line. All primary flow field features are seen to be captured extremely well by the computational solution. Shock location and curvature are almost identical, expansion lines on the shoulder are located at the proper positions and angles, and recompression shocks emanating from the windshield are matched exactly. Also evident in the density contours of Figure 12 is the aforementioned flow disturbance on the lower, windward surface of the tension cone model.

a) **Axial force coefficient, C_A**
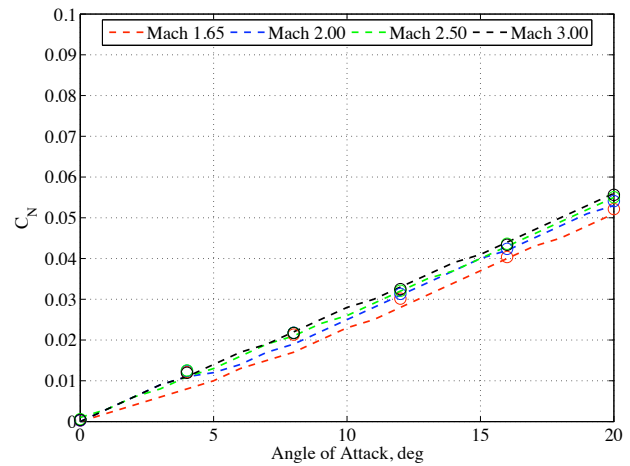
b) **Normal force coefficient, C_N**
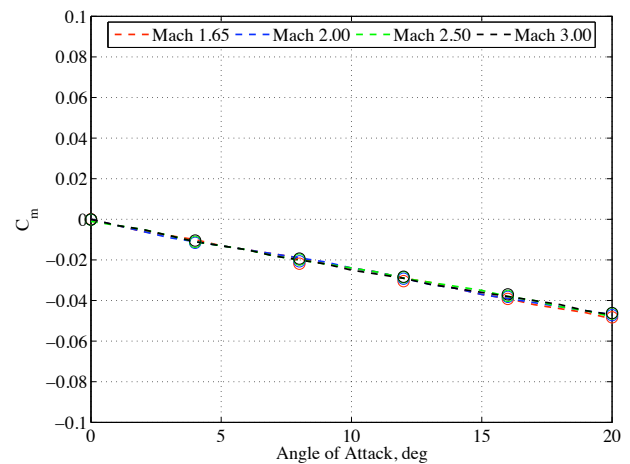
c) **Pitching moment, C_m**

Figure 11. Comparison of CFD and measured force and moment coefficients. Note: circles correspond to Overflow solutions.
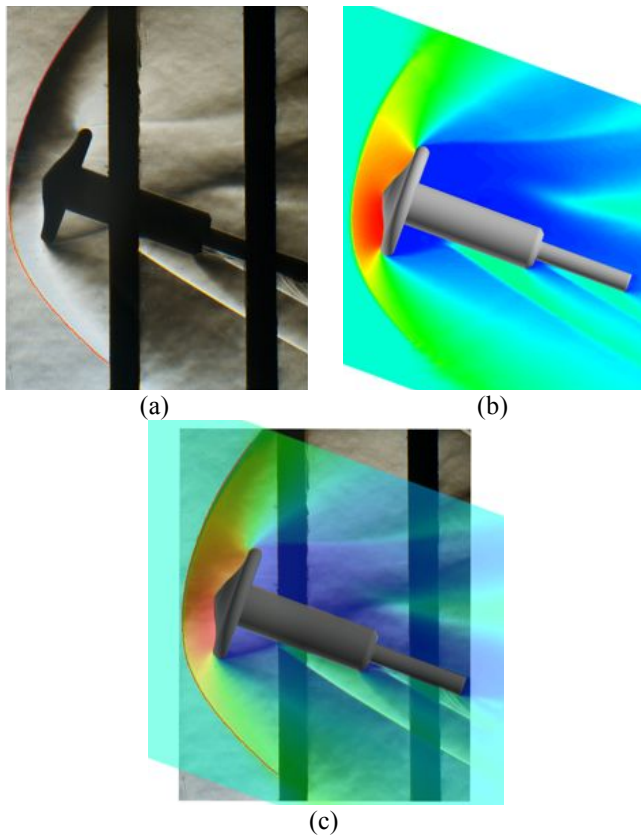
(a)

(b)

(c)

Figure 12. Comparison of shock structure at a 20° angle of attack for Mach 2.0 and Re = 10⁶.

[1] From the results shown, it can be seen that the viscous computational analysis is capable of accurately modeling the physics of the flow field at lower Mach numbers. With this in mind, the computational solutions can be used to garner insights into flowfield features that could not be observed during testing. For example, **Figure** 7 shows a small rise is drag coefficient as Mach number is increased to about 2.5 or 3.0 after which the drag decreases again. Examination of the surface pressure data shows that this rise in drag is due to a lag in the aft body pressure. That is, as Mach is increased, pressure coefficients on the forebody and aftbody begin to rise. However, the rise in aftbody pressure initially occurs more slowly than the rise in forebody pressure and thus greater drag is produced. Provided in Figure 13 is a sequence of solutions showing the contraction of the recirculation region behind the tension cone as Mach number is increased. Between Mach 1.65 and Mach 2.00 the bow shock is seen to move substantially closer to the forebody while the recirculation region shows only moderate contraction. Subsequent increases in Mach number provide greater closure of the recirculation zone until at Mach 3.0 the zone is nearly touching the back end of the windshield. The rise in base pressure can be correlated to the progression of the core of the recirculation region moving closer to the back of the tension cone [12].
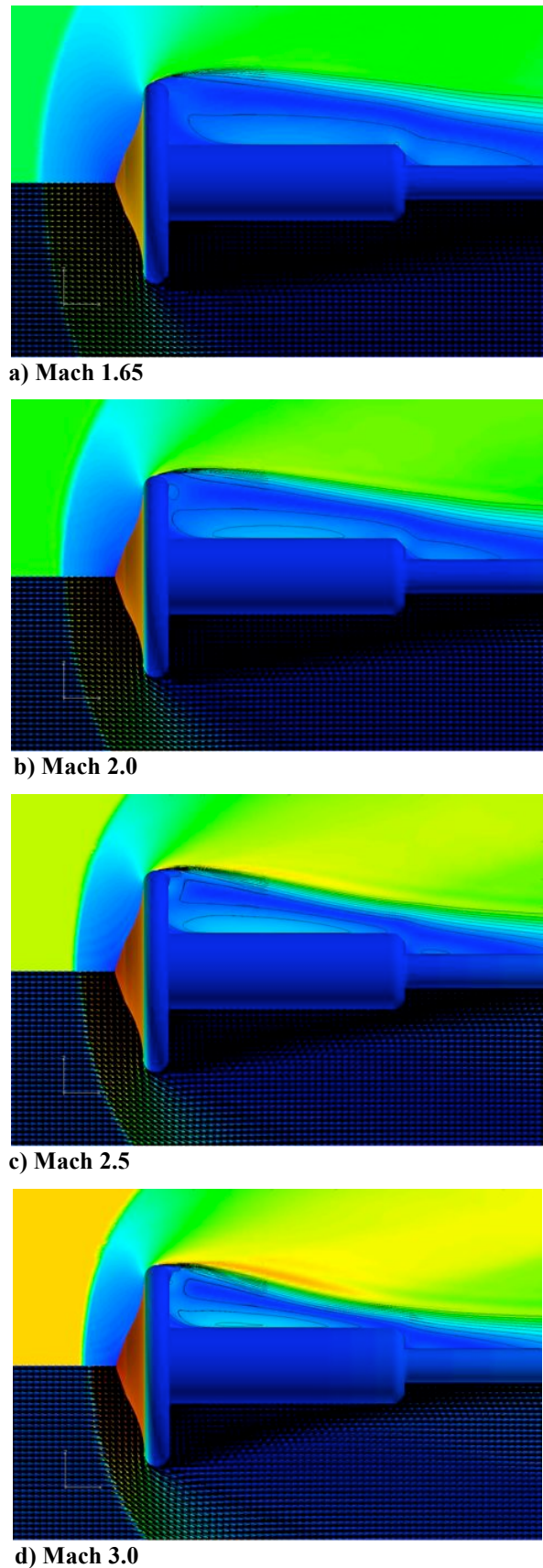

a) Mach 1.65

b) Mach 2.0

c) Mach 2.5

d) Mach 3.0

Figure 13. Mach contours and velocity fields with increasing Mach number.

8

5. TENSION CONE SHAPE CHARACTERIZATION

The outer mold line of the tension cone is a combination of the assumed forebody (entry vehicle) geometry, the curvature of the tension shell portion, and the inflatable torus. Although the tension shell portion is derived on the basis of a given pressure distribution, there are several parameters that control the final configuration. These include the attachment angle between the aeroshell and tension shell, the size of the torus, and the overall size of the tension cone. Understanding the influence of these parameters on the drag performance of a tension cone is important for future development efforts. Thus, a study was undertaken with the objective of providing drag estimates for a broad range of tension cone configurations. A secondary objective entailed an examination of flowfield features that may prove detrimental to flexible tension cones.

Scope

To assist in rapid evaluation of a large number of tension cone configurations, several simplifications were made. First, the pressure distribution was assumed to be Newtonian. The assumption of a Newtonian pressure distribution allows for an analytical formulation of the tension shell curvature. Although this is a poor approximation of the actual surface pressure distribution, prior studies have observed that the difference in curvature between a tension shell derived on the basis of a Newtonian pressure distribution and one derived from actual pressure distributions is relatively small [4].

The aerodynamic analysis was performed using NASCART-GT. As before, solutions were generated for inviscid, axisymmetric flow. Though this approach does not provide the accuracy seen by the Overflow solutions, it does allow for rapid analysis of multiple geometries and should be sufficient to capture significant trends in aerodynamics.

A total of 120 different tension cone geometries were analyzed by varying three main parameters. Using the nomenclature shown in Figure 14, these include the tension shell attachment angle (θ_{tc}), the ratio of tension cone reference area to aeroshell reference area, and the ratio of tension shell radius to torus radius (r_{ts}/r_t). The forebody was a 70° sphere cone.
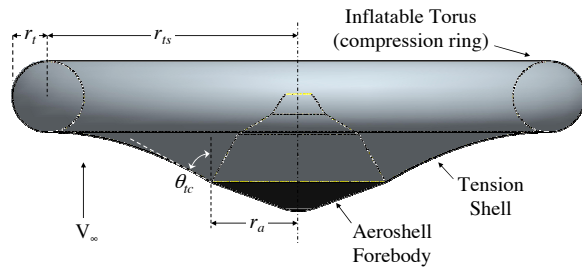

Figure 14. Tension cone configuration nomenclature.

The range of shape parameters considered is provided in Table 1. All solutions were computed for a Mach 5 condition is a Mars-like atmosphere ($\gamma = 1.33$).

Table 1. Summary of shape parameter range evaluated.

Parameter	Min Value	Max Value
Attachment Angle, θ_{tc}	40	70
Area Ratio, $(r_b + r_t)^2/r_a^2$	5	30
Torus Ratio, r_{ts}/r_t	5	13

Approach Validation

A stated secondary objective was the characterization of flowfield features that would be detrimental to a flexible body. In particular, prior testing of rigid tension cone configurations demonstrated the possibility of nested shocks on the tension shell [3]. Often, this led to a region of unsteady, separated flow immediately behind the shock. This was mitigated as the cone angle of the tension shell was increased and the shock became fully detached.

Although the direct cause of the flow separation was likely the presence of embedded shocks within the boundary layer, these were closely tied to the presence of the attached shock on the tension shell. An inviscid code would not be able to resolve the embedded shocks, but should still be able to predict nested shocks to varying degrees. Verification of this was sought by performing CFD analyses on geometries and conditions similar to those for which the nested shocks were observed. A qualitative comparison of the flow fields was then made using Schlieren images available from those tests. The results of this comparison are provided in Figure 15.
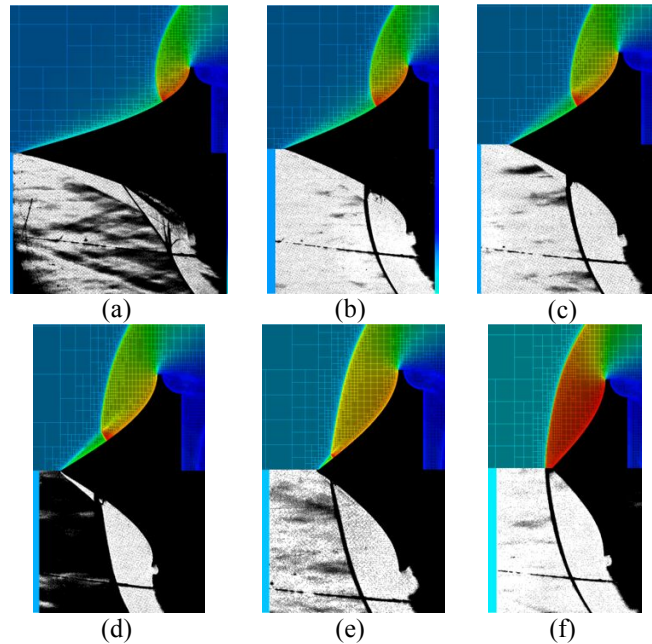

(a) (b) (c)

(d) (e) (f)

Figure 15. Comparison of inviscid CFD and Schlieren images at Mach 3.0 for tension cones with half angles of (a) 15.8°, (b) 21.5°, (c) 27.0°, (d) 31.8°, (e) 38.3°, and (f) 47.0°. Schlieren images adapted from [3].

9

For the shallower cone angles, the flowfields are more complex and several embedded shocks can be seen. However, the general location of the nested shock on the tension cone is matched by the inviscid CFD. Flowfield matching can be seen to improve as the cone angles are increased. For cone angles exceeding 31º, the inviscid CFD captures the oblique shock from the tip, the location of the nested shock, and the overall curvature of the nested shock. The CFD is also seen to accurately predict the point at which the shock becomes fully detached, shown in Figure 15f.

A comparison of the computed drag coefficients is provided in Figure 16. As before, the forebody-only drag coefficients more closely match the measured drag coefficients. Furthermore, with the exception of the two lowest cone angles, the predicted forebody-only drag is within 5% of the measured value.
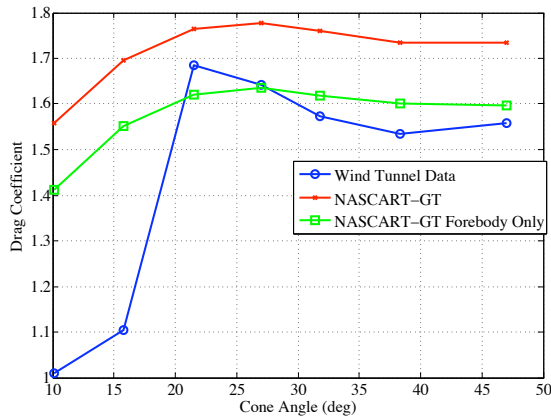

Figure 16. Comparison of computed drag coefficients for validation tension cone models.

Results

For the four tension shell interface angles evaluated (40º, 50º, 60º, and 70º), only geometries with a 40º interface angle were seen to develop shocks attached to the tension shell surface. A summary of the area ratios and torus ratio's for which this occurred is provided in Figure 17. In particular, geometries with area ratios exceeding 20 consistently produced attached shocks. Geometries with area ratios less than 20 often showed transitional behavior where interactions were seen between a detached bow shock and a tension shell shock, though the tension shell shock did not reach the surface. An example of this progression, from fully detached to fully attached is provided in Figure 18. Smaller tori (larger values of r_{ts}/r_t) were also observed to be more likely to produce attached shocks.
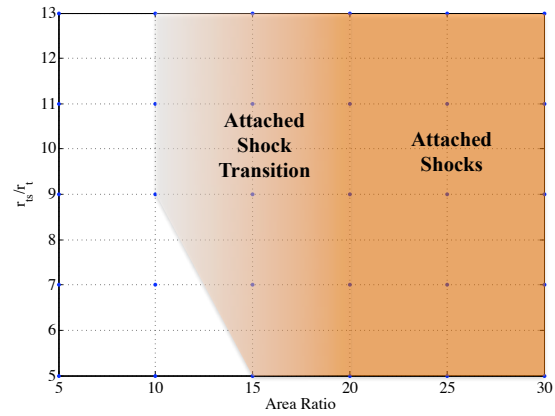

Figure 17.   Shape parameters resulting in attached shocks for a 40º tension shell attachment angle.
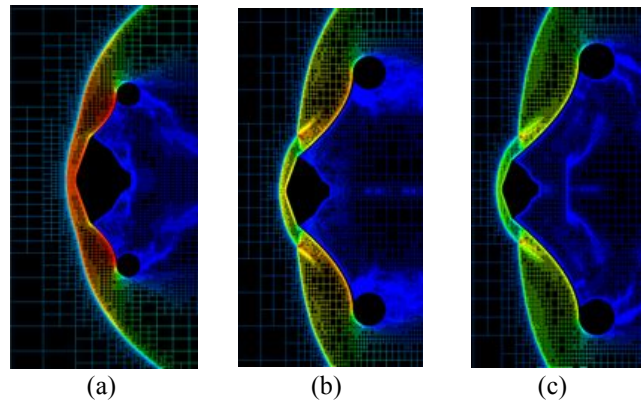

Figure 18. Development of attached shock for geometries with a 40º interface angle, torus ratio of 7, and area ratio of (a) 5, (b) 15, and (c) 25.

Contours of forebody-only drag coefficient are provided in Figure 19. Of note, geometries with a 40º tension shell interface angle generally produced more drag than geometries with steeper angles. This can be attributed to the presence of the attached shock. The attached shock sits closer to the tension cone and provides a greater pressure recovery, thus increasing the surface pressure behind it.

Aside from the 40º cases, drag coefficients are seen to vary little with interface angle. Drag is also seen to be relatively insensitive to area ratio, particularly for area ratios of 10 or more. Of the three geometry parameters, it is the size of the torus that appears to have the greatest impact on drag coefficient. Smaller tori produce larger drag coefficients, though variation is still less than 10% overall. As the torus size decreases, the sonic line moves further outboard and greater pressure recovery is seen on the periphery of the tension cone.
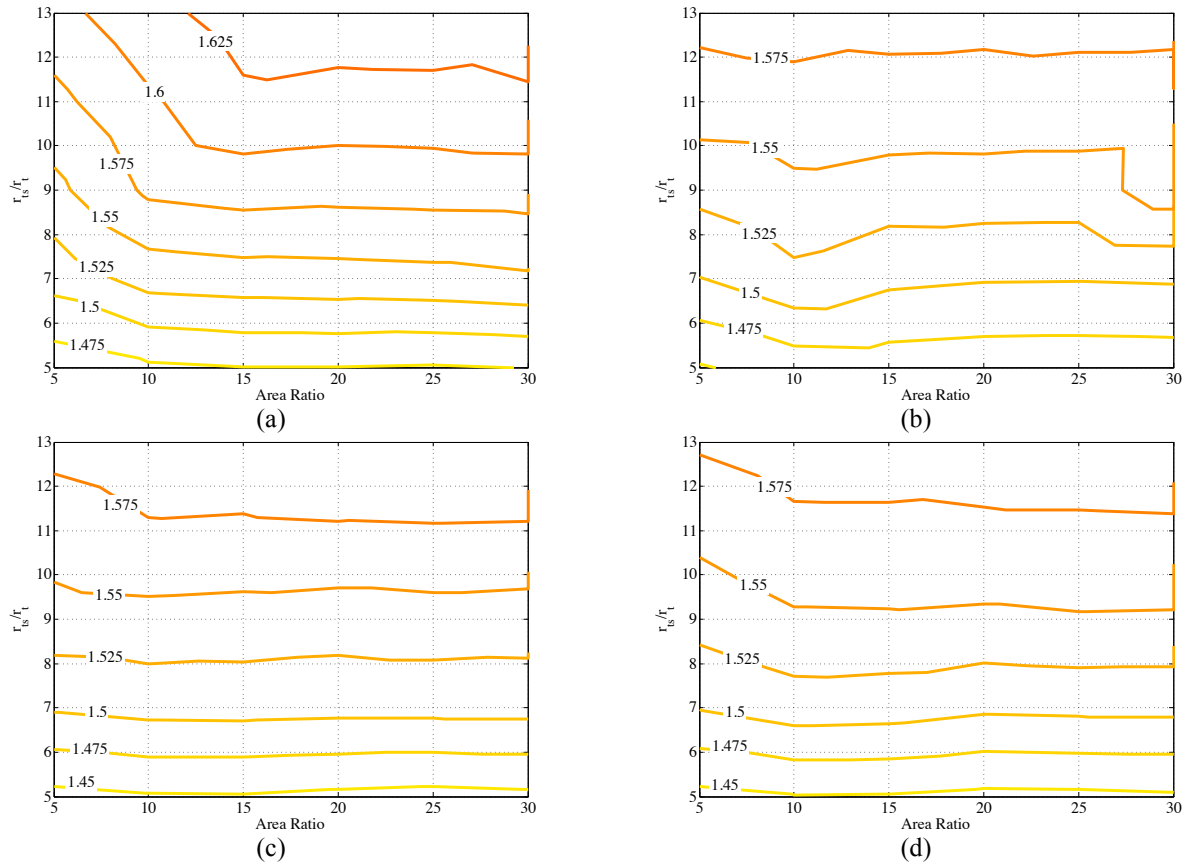
Figure 19. Contours of forebody-only drag coefficient for tension shell interface angles of (a) 40º, (b) 50º, (c) 60º, (d) 70º.

6. CONCLUDING REMARKS

The objective of this research was to characterize the capability of computational fluid dynamic codes of varying fidelity to accurately model the static aerodynamic performance of a tension cone IAD. Lower fidelity inviscid and axisymmetric solutions were generated and compared against pressure and force and moment data acquired during testing of a rigid tension cone IAD. Predictions of surface pressure distribution across the forebody were shown to be in reasonable agreement with the wind tunnel data while aftbody pressures tended to be under predicted. Calculated drag coefficients were within 10% of the measured values, with better agreement attained when only forebody pressures were considered. These results demonstrated the suitability for using inviscid aerodynamic calculations for rapid, conceptual trades of supersonic tension cone IADs.

Solutions attained using a viscous, Navier-Stokes solver demonstrated much excellent agreement with test data at Mach numbers up to 3.0. However, instability and separation in the flow was calculated for Mach numbers of 3.5 and above, contrary to the results of the wind tunnel test program. This is likely due to the inability of the turbulence model to accurately predict transition to turbulent flow. Predictions of static force and moment coefficients were also seen to match well with experimental data.

A parametric sweep of tension cone configurations was performed using inviscid, axisymmetric calculations. The results from this trade provide an initial indication of the drag performance and flow stability bounds of the tension cone trade space. Assuming a 70º sphere-cone forebody, tension cones with interface angles of 50º or greater were calculated to not exhibit attached shocks and had similar drag performance.

11

REFERENCES

[1] R. D. Braun and R. M. Manning, "Mars Exploration Entry, Descent, and Landing Challenges," *Journal of Spacecraft and Rockets*, vol. 44, no. 2, pp. 310-323, March-April 2007.

[2] I. G. Clark, A. L. Hutchings, C. L. Tanner, and R. D. Braun, "Supersonic Inflatable Aerodynamic Decelerators For Use On Future Robotic Missions to Mars," IEEE AC-1419, IEEE Aerospace Conference, Big Sky, MT 2008.

[3] W. D. Deveikis and J. W. Sawyer, "Aerodynamic Characteristics of Tension Shell Shapes at Mach 3.0," NASA Technical Note TN D-5816, May 1970.

[4] J. W. Sawyer, "Effects of Pressure Distributions on Bluff Tension-Shell Shapes," NASA Technical Note TN D-5636, February 1970.

[5] J. C. South Jr., "Calculation of Axisymmetric Flow Past Blunt Bodies With Sonic Corners, Including a Program Description and Listing," NASA Technical Note TN D-4563, May 1968.

[6] S. Z. Tu and S. M. Ruffin, "Calculation of Nonequilibrium Flows Using a Solution Adaptive, Unstructured Cartesian-Grid Methodology," AIAA Paper 2002-3098, April 2002.

[7] S. Z. Tu and S. M. Ruffin, "Solution Adaptive, Unstructured Cartesian-Grid Methodology for Chemically Reacting Flow," AIAA Paper 2002-3097, April 2002.

[8] R. H. Nichols and P. G. Buning, "User's Manual for OVERFLOW 2.1," August 2008.

[9] M. E. Olsen and T. J. Coakley, "The Lag Model, a Turbulence Model for Non-Equilibrium Flows," AIAA Paper 2001-2564, July 2001.

[10] M. E. Olsen, R. P. Lillard, and T. J. Coakley, "The Lag Model Applied to High Speed Flows," AIAA Paper 2005-101, February 2005.

[11] N. M. Chaderjian and M. E. Olsen "Grid Resolution and Turbulence Model Effects on Space Capsule Navier-Stokes Solutions," AIAA Paper 2007-4562, 2007.

[12] I. M. Jaremenko, "Wakes, Their Structure and Influence Upon Aerodynamic Decelerators," NASA Contractor Report CR-748, April 1967.

BIOGRAPHY

Ian Clark *is a PhD candidate at the Georgia Institute of Technology, where he also received his BS and MS. Ian's current research involves developing and maturing inflatable aerodynamic decelerators (IADs) for use during atmospheric entry. As part of this research, he has worked on conceptual IAD system design, entry flight mechanics trades, and the development of fluid-structure interaction codes capable of predicting the behavior of flexible decelerators. Presently, Ian is a research engineer on a series of supersonic wind tunnel tests of a candidate IAD configuration.*

Robert Braun *is an Associate Professor in the Guggenheim School of Aerospace Engineering at the Georgia Institute of Technology. As Director of Georgia Tech's Space Systems Design Laboratory, he leads a research program focused on the design of advanced flight systems and technologies for planetary exploration. He is responsible for undergraduate and graduate level instruction in the areas of space systems design, astrodynamics and planetary entry. Prior to coming to Georgia Tech, Dr. Braun worked at NASA Langley Research Center for sixteen years where he contributed to the design, development, test, and operation of several robotic space flight systems. Dr. Braun is an AIAA Fellow and the principal author or co-author of over 150 technical publications in the fields of planetary exploration, atmospheric entry, multidisciplinary design optimization, and systems engineering.*